J. Fluid Mech. (1987), *vol.* 182, *pp.* 427–446
Printed in Great Britain

Similarity solutions for stratified rotating-disk flow

By J. D. GODDARD, J. B. MELVILLE† AND K. ZHANG
Department of Chemical Engineering, University of Southern California,
Los Angeles, CA 90089-1211, USA

(Received 20 May 1986 and in revised form 3 February 1987)

This work treats the vertically stratified system of two homogeneous fluid layers confined between horizontal infinite rotating disks which rotate steadily about a common vertical axis. Allowance is made for uniform injection of fluid at either disk. With appropriate restrictions on disk rotational speeds and injection rates a flat interface is possible, and the problem admits similarity solutions to the Navier–Stokes equations of the Kármán–Bödewadt–Batchelor variety. This type of flow allows for a uniformly accessible surface of interphase mass and heat transfer at the two-fluid interface, and, with that as the primary motivation, the present work provides exploratory numerical solutions of the above equations for both corotation and counter-rotation combined with injection.

A linearized theory is given for the case of nearly rigid rotation, with explicit analytical results for the large-Reynolds-number boundary-layer limit. Also, we offer a theoretical discussion of the inviscid limit for arbitrary rotation and injection rates. Based on the type of Euler-cell solutions identified in previous work, we derive the remarkably simple formula

$$\rho_1 \omega_1^2 \cot^2 \frac{\omega_1 d_1}{V_1} = \rho_2 \omega_2^2 \cot^2 \frac{\omega_2 d_2}{V_2}$$

connecting densities ρ, depths d, rotation speeds ω and injection velocities V.

Sample calculations and comparisons are given for property ratios typical of water–kerosene layers. In this case, the linearized theory works exceedingly well for corotation with small injectional Rossby numbers $V/\omega d$. The simple inviscid theory cited above shows excellent agreement with the numerical computations for Reynolds numbers greater than 500 and for Rossby numbers $> 1/\pi$, corresponding to strong blowing in the inviscid regime. The larger-wavelength inviscid cell structure appears to provide the kind of stagnation-flow pattern essential to the application envisaged.

1. Introduction

Uniformly accessible surfaces, that is, surfaces having uniform mass or heat transfer coefficients, are especially useful for the study of various physicochemical processes that accompany laminar forced convection. Based on the pioneering work and treatise of Levich (1962), the classical Kármán flow (Kármán 1921) near a solid rotating disk has served for many years as a standard laboratory device in the study of chemical reaction kinetics at fluid–solid interfaces, especially in the field of electrochemistry. For this purpose Pollard & Newman (1980) have proposed a generalization of the Kármán–Levich theory to cover the case of continuously stratified flows having vertical (disk-normal) property variations.

† Now at the Naval Ocean Systems Center, Code 634B, San Diego, CA 92152-5000, USA.

In a related work, with objectives and basic equations closer to those of the present paper, Pécheux & Boutin (1985) have considered the case of discrete stratification, involving two fluids confined between infinite rotating disks. As they point out, an apparatus based on this flow configuration has the potential for generating a uniformly accessible interface between immiscible fluids, an idea that provides much of the motivation for the present work (cf. Melville & Goddard 1985). Unfortunately, most of the hydrodynamic systems proposed to date, such as those considered by Stowe & Shaeiwitz (1981) along with their own stratified flow between rotating disks, involve non-uniform interfaces. One possibility is suggested by stagnation flow without rotation, which has already been proposed as an alternative to the Kármán flow by Ghim & Chang (1983) for fluid–solid interfaces. In the case of fluid–fluid interfaces, the stagnation flow between opposing streams such as impinging liquid jets comes immediately to mind and has been analysed by Chapman & Bauer (1975) for two streams of the same fluid. As will become more apparent in the following discussion of immiscible streams having different properties, the upstream approach velocities cannot be prescribed independently if the interface is to remain flat.

In general, the primary requirements for a uniformly accessible surface for passive-scalar transport are: (*a*) a surface-normal fluid velocity which depends only on an appropriate normal coordinate, measuring (curvilinear) distance from the surface, and (*b*) uniform boundary conditions on the concentration or potential fields that govern diffusion and convection. Even when condition (*a*) is satisfied it is not always easy to realize condition (*b*), as illustrated by the work of Smith & Colton (1972) on the so-called Bödewadt or 'teacup' flow in which the disk is stationary and the fluid rotates uniformly far away.

As shown by Bödewadt (1940) and later elucidated further by Batchelor (1951), centrifugal suction caused by the far-field rotation leads to a flow directed inwards toward the disk axis and upwards away from the disk (that is, a flow having negative radial or r-velocity and positive vertical or z-velocity). The inward radial velocity leads almost inevitably to an edge effect associated with the developing concentration layer on any real surface of finite extent; or else it implies a trivial concentration field, uniform throughout the system.

From the preceding considerations, one concludes that for rotationally driven flows a Kármán-type or 'centrifugal-fan' (Batchelor 1951) flow pattern with radial outflow near the transfer surface will in practice be necessary for the elimination of edge effects. There remains, therefore, a challenging question not fully explored by Pécheux & Boutin (1985) as to how one might generate the requisite flow field. For disk flow without injection, this appears to require an interface that rotates more rapidly than the adjacent bodies of fluid. While the numerical study of Keller & Szeto (1980) indicates that such a flow structure can arise near the mid-plane in the similarity flow of a homogeneous fluid,† we have not been able to generate such structures numerically in the present work. On the other hand, it will be shown presently that the desired flow pattern can in principle be generated at arbitrary Reynolds number by a judicious combination of rotation and fluid injection at the disks, such as might be achieved by employing porous disks. This stratagem enables one to counterbalance the centrifugally induced (positive) radial pressure gradients arising from rotation against the (negative) gradients associated with the interfacial stagnation flow generated by injection.

† We are indebted to a referee for pointing this out to us.

To clarify certain of the above issues, we report here on some exploratory numerical finite-difference solutions to the Kármán–Bödewadt–Batchelor (KBB) similarity form of the Navier–Stokes equations. As a partial test of the numerics and a guide to understanding, we also develop a linear theory for nearly-rigid rotation and an inviscid theory for the large-Reynolds-number cell structure and multiplicity. Given the possibilities for application, we hope to make a case here for more detailed studies of some of the interesting fluid mechanics related to the large-Reynolds-number structure (Kuiken 1971; Dijkstra 1980; Zandbergen & Dijkstra 1987), multiplicity (Holodniok, Kubiček & Hlavaček 1977, 1981; Lai, Rajagopal & Szeri 1984) and edge effects (Brady & Durlofsky 1987), which have received considerable attention with respect to the related problem of homogeneous fluids.

2. Analysis

We consider now the flow between infinite parallel planes of two immiscible, constant-property Newtonian fluids having respective densities, viscosities and kinematic viscosities denoted by ρ_1, μ_1, ν_1 and ρ_2, μ_2, ν_2. Fluid 1 occupies the region $0 \leqslant z \leqslant d_1$ and fluid 2 the region $-d_2 \leqslant z \leqslant 0$, with

$$d = d_1 + d_2 \tag{2.1}$$

denoting the plate spacing. The upper and lower boundaries at $z = d_1, -d_2$ are imagined to consist of porous solid plates, at which there may exist non-zero normal velocities together with zero tangential slip of the fluids. Furthermore, the bounding plates are assumed to execute rigid-body rotations about a common (z) axis, with angular velocities denoted by ω_1 and ω_2, respectively.

We are concerned here with steady and axisymmetric (KBB) similarity solutions to the Navier–Stokes equations, of the type discussed by many previous investigators, in which the normal velocity component w depends only on z (Batchelor 1951). We adopt the dimensionless forms of Lance & Rogers (1962) with, now, two sets of equations of the form

$$\left.\begin{aligned} u = r\omega F(\xi), \quad v = r\omega G(\xi), \quad w = (\nu\omega)^{\frac{1}{2}} H(\xi) \\ \text{and} \qquad p = \rho\nu\omega P(\xi) + \rho\omega^2 C_2^1 r^2, \end{aligned}\right\} \tag{2.2}$$

where F, G and H satisfy

$$\left.\begin{aligned} F''' &= R_i^{\frac{1}{2}} HF' + R(F^2 - G^2 + C), \\ G'' &= R_i^{\frac{1}{2}} HG' + 2RFG, \\ H' &= -2R_i^{\frac{1}{2}} F, \end{aligned}\right\} \tag{2.3}$$

together an equation for $P(\xi)$ in terms of H and F. Here

$$\xi = \frac{z}{d}, \quad R = \frac{\omega d^2}{\nu} \tag{2.4}$$

denote a dimensionless vertical coordinate and a Reynolds number based on some characteristic angular velocity or frequency ω. In fluid i the quantities ρ, ν, R and the constant C in (2.2) and (2.3) take on values ρ_i, ν_i, R_i, C_i respectively, for $i = 1, 2$.

The boundary conditions at the upper and lower plates are, then,

$$\left.\begin{aligned} &F = 0, \quad G = \gamma_1 \equiv \frac{\omega_1}{\omega}, \quad H = H_1 = \eta_1 R_1^{\frac{1}{2}}, \quad \text{at } \xi = \xi_1 \equiv \frac{d_1}{d}, \\ \text{and} \\ &F = 0, \quad G = \gamma_2 \equiv \frac{\omega_2}{\omega}, \quad H = H_2 = \eta_2 R_2^{\frac{1}{2}}, \quad \text{at } \xi = \xi_2 \equiv -\frac{d_2}{d}. \end{aligned}\right\} \tag{2.5}$$

In addition, the matching of velocity and stress on the stationary flat interface requires the continuity of ρC, F, G, $(\nu)^{\frac{1}{2}}H$, $\mu F'$ and $\mu G'$, with $H = 0$, at $\xi = 0$. We note that, with the scaling implied in (2.2) and (2.5), the parameters η_1 and η_2 represent in effect Rossby numbers since they have the form $V/\omega d$. By expressing the boundary values of H in terms of η we have anticipated the fact that the Rossby number must be taken as $O(1)$ or larger if injection is to play a significant role for large Reynolds number.

We further note that the contributions to pressure arising from gravity and interfacial tension are not operative as long as the interface is presumed flat, a condition that requires the interfacial matching of radial pressure gradients and, hence, of the quantity ρC. As discussed above, the requirement of a flat interface appears necessary to the attainment of similarity solutions with uniformly accessible interface, at least for finite values of d. The parameter ω in (2.4) is free and, for the sake of discussion here and for the numerical analysis below, we shall specify it here as follows:

(a) for non-zero rotation ($\omega_2 \neq 0$),

$$\omega = \omega_2, \quad \gamma_2 \equiv 1 \tag{2.6}$$

or (b) for zero rotation ($\omega_1 = \omega_2 = 0$),

$$\omega = \frac{V_2}{d}, \quad \gamma_1 = \gamma_2 = 0, \tag{2.7}$$

where V_2 is the injection velocity at $\xi = \xi_2$.

Given the order of the system of differential equations (2.3), the number of subsidiary conditions implied by (2.5)–(2.7) and the above internal matching conditions at $\xi = 0$, we conclude that four of the five quantities $\xi_1 \equiv 1 + \xi_2, \gamma_1, \gamma_2, \eta_1$ and η_2 in (2.5)–(2.6) can be considered free parameters, once the fluid properties and disk spacing d are specified. In the present work we consider the relative fluid depths and, hence, ξ_1 to be fixed leaving three free parameters. This is to be contrasted to the work of Pécheux & Boutin (1985) where injection is absent ($\eta_1 = \eta_2 \equiv 0$) and ξ_1 is determined by fixing both disk rotations γ_1 and γ_2. In this regard, we note two extreme cases which are of interest here: (i) rotational flows, without injection ($\eta_1 = \eta_2 = 0$) and (ii) stagnation flows, without rotation ($\gamma_1 = \gamma_2 = 0$).

In Case (i), with $\gamma_2 \equiv 1$, the parameter γ_1 must be determined by the solution to the above equations. In other words, the requirement of a flat interface dictates that the rotational speed of one plate be dependent on that of the other. One can better appreciate this state of affairs by considering the limit of an unbounded flow field where d_1 and d_2 are infinite. In this case, the matching of the radial pressure gradients induced by the far-field rotations at $z = \pm\infty$ requires that

$$\rho_1 \omega_1^2 = \rho_2 \omega_2^2, \quad \text{i.e. } \gamma_1 \equiv \frac{\omega_1}{\omega_2} = \pm \left(\frac{\rho_2}{\rho_1}\right)^{\frac{1}{2}}. \tag{2.8}$$

As with finite d, we may have counter-rotation or corotation of the disks, corresponding to $\gamma_1 < 0$ or $\gamma_1 > 0$, respectively.

The unbounded flow gives rise formally of course to infinite Reynolds number R in (2.4), leading one to anticipate a boundary-layer structure near the interface, or at other viscous interlayers (Batchelor 1951), where another coordinate becomes appropriate in (2.3). Early in the present study we made several unsuccessful attempts, for the unbounded flow with boundary conditions (2.8), to generate numerical solutions exhibiting a (Kármán) centrifugal-fan structure with radial outflow near the interface in both fluids. Based on this exploratory numerical work and Batchelor's (1951) exhaustive discussion for homogeneous fluids, we conclude that a Kármán-type flow pattern in a viscous interlayer or interfacial region may be difficult to attain for stratified fluids in Case (i) above, pure rotation. This conclusion does not of course rule out the appearance of such flow patterns in restricted regions of parameter space, as indicated by the work of Keller & Szeto (1980) for homogeneous fluids and as faintly evident in some of our own solutions for stratified flow presented below (e.g. figure 2 at $R_1 = 10$).

In Case (ii) above, with $\omega_1 = \omega_2 = 0$, the matching of stagnation pressure fields requires that η_1 and η_2 be interrelated, so that upper and lower injection velocities cannot be prescribed independently. Here, we anticipate the classical, unbounded stagnation flow in the limit $d_1 \to \infty$ and $d_2 \to \infty$, provided η_1 and η_2 remain finite for $R_1 \to \infty$ and $R_2 \to \infty$ in (2.5). In this case the matching of radial pressure gradients requires a condition of the form (2.8), where now ω_1 and ω_2 denote far-field strain rates associated with non-rotating stagnation flows.

In the general case, we can have a mixed-type flow with both injection and rotation at the disks, which we believe could simulate the effects of axial impellers or porous disks in a real laboratory apparatus. From the point of view of attaining a uniformly accessible interface, the combination of injection and rotation confers an additional degree of freedom over the extremes of Cases (i) and (ii) cited above.

Given the well-known complexity of either Case (i) or (ii) above, we can anticipate that the intermediate cases will require numerical solution methods. One notable exception is the case of corotating disks with nearly equal fluid densities and weak injection. In this case, which we consider now, we have a nearly rigid rotation of the type envisaged by Proudman (1956), Stewartson (1957) and Hocking (1962), whose linearized equations would also apply to finite container geometries and flows that do not have the similarity form. Since we are, however, primarily interested here in the latter, we can perform the linearization directly on the reduced equations (2.3).

3. Nearly rigid rotation

To simplify presentation of the linearized theory, we cast (2.3)–(2.5) into a simpler form that is especially appropriate for large Reynolds number R. Employing the standard (Kármán) scaled coordinate

$$\zeta = \xi R^{\frac{1}{2}} = z\left(\frac{\omega}{\nu}\right)^{\frac{1}{2}}, \tag{3.1}$$

we adopt a complex dependent variable,

$$f'(\zeta) = F + \mathrm{i}G, \quad \text{with } H = -2\,\mathrm{Re}\,(f), \tag{3.2}$$

so that (2.3) becomes

$$f''' + 2\,\mathrm{Re}\,(f) f'' - C - f'^2 = 0, \tag{3.3}$$

where primes denote derivatives with respect to ζ and where Re denotes the real part of a complex quantity. Equations of the above type apply of course in each of our two fluids, with $f \equiv f_i(\zeta_i)$, $\zeta_i \equiv z(\omega/\nu_i)^{\frac{1}{2}}$, and $C \equiv C_i$, etc., for $i = 1, 2$, respectively.

It will be noted that (3.3) represents a kind of complex Falkner–Skan equation (Schlichting 1975) and suggests a certain mathematical kinship amongst various similarity-type flows. For the present application, the boundary conditions (2.5) and the interfacial matching conditions can easily be written as conditions on $f(\zeta)$ at $\zeta_1 = \xi_1 R_1^{\frac{1}{2}}$, $\zeta_2 = \xi_2 R_2^{\frac{1}{2}}$ and $\zeta_1 = \zeta_2 = 0$ respectively.

For the case of nearly rigid rotations, we specify the rotation ω in (2.2)–(2.5) and (3.1), together with an associated small parameter ϵ, by

$$\omega = \tfrac{1}{2}(\omega_1 + \omega_2), \quad \epsilon = \frac{\omega_1 - \omega_2}{\omega}. \tag{3.4}$$

As perturbation series for small ϵ, we then take

$$f'(\zeta) = \mathrm{i} + \epsilon\phi(\zeta) + O(\epsilon^2), \tag{3.5}$$

$$H(\zeta) = -2\epsilon \operatorname{Re}\left\{\int_0^\zeta \phi(s)\,\mathrm{d}s\right\} + O(\epsilon^2), \tag{3.6}$$

$$C = 1 + \alpha\epsilon + O(\epsilon^2), \tag{3.7}$$

$$\eta R^{\frac{1}{2}} = \beta\epsilon + O(\epsilon^2), \tag{3.8}$$

etc., where two distinct sets of $O(1)$ quantities $\phi_i, \zeta_i, \alpha_i, \beta_i$, etc., for $i = 1, 2$, are implied. The scaling adopted in (3.8) is intended to convey the understanding that η_1 and η_2, the Rossby numbers based on the disk-normal injection velocities, must be $O(\epsilon)$ for the present theory to hold.

With the above conventions, (3.3) gives for terms of $O(\epsilon)$

$$\phi'' - 2\mathrm{i}\phi = \alpha, \tag{3.9}$$

whose general solution is

$$\phi = A\,\mathrm{e}^{(1+\mathrm{i})\zeta} + B\,\mathrm{e}^{-(1+\mathrm{i})\zeta} + \tfrac{1}{2}\mathrm{i}\alpha, \tag{3.10}$$

where A and B are complex constants.

Letting, as before subscripts $i = 1, 2$ refer to the upper and lower fluids, respectively, two distinct expressions of the above type apply in the regions $\zeta = \zeta_1 \geqslant 0$ and $\zeta = \zeta_2 \leqslant 0$, and application of the requisite boundary and interfacial matching conditions leads to the equations

$$A_1 + B_1 + \tfrac{1}{2}\mathrm{i}\alpha_1 = A_2 + B_2 + \tfrac{1}{2}\mathrm{i}\alpha_2, \tag{3.11}$$

$$A_1 - B_1 = \lambda(A_2 - B_2), \tag{3.12}$$

where $$\lambda = \left(\frac{\rho_2 \mu_2}{\rho_1 \mu_1}\right)^{\frac{1}{2}}$$

and

$$E_k A_k + E_k^{-1} B_k + \tfrac{1}{2}\mathrm{i}\alpha_k = (-)^{k+1}\tfrac{1}{2}\mathrm{i}, \tag{3.13}$$

$$\operatorname{Re}\{(1-\mathrm{i})[A_k(E_k - 1) - B_k(E_k^{-1} - 1)]\} = -\beta_k \tag{3.14}$$

where $$E_k = \exp\{(1+\mathrm{i})\xi_k R_k^{\frac{1}{2}}\} \quad \text{for } k = 1, 2$$

together with

$$\rho_1(1 + \alpha_1\epsilon) = \rho_2(1 + \alpha_2\epsilon), \tag{3.15}$$

which, we recall, arises from the interfacial matching of radial pressure gradients through the term ρC.

The latter condition dictates of course that the density differences must be $O(\epsilon)$ or, equivalently, by (3.15) and (3.4), that

$$\frac{\rho_1-\rho_2}{\rho_2\alpha_2-\rho_1\alpha_1}=2\left(\frac{\omega_1-\omega_2}{\omega_1+\omega_2}\right). \tag{3.16}$$

The rotation ratio, $\omega_1/\omega_2\sim 1$, is thus directly tied to density ratio, $\rho_1/\rho_2\sim 1$, once α_1 and α_2 are known. The latter, which are (real) constants, together with the (complex) constants $A_k, B_k, k=1,2$, could be determined from the (six complex or ten real) equations (3.11)–(3.14), if the (real) injection parameters β_k and the parameters E_k were specified. However, the E_k involve ω_1 and ω_2, of which one is unknown and connected to the other through (3.16), which of course involves the unknowns α_1 and α_2. This in effect renders the problem nonlinear.

Although the set (3.11)–(3.14) is linear algebraic in form, we have not taken the trouble to work out an explicit analytical solution. The latter would doubtless be so complicated in form that, given the above nonlinearities, its use for computation would scarcely be easier than the direct numerical solution of (3.11)–(3.14) and (3.16), which we have chosen to employ here for general values of the Reynolds number.

In the special case of large Reynolds numbers, where $|E_1|\gg 1$ and $|E_2|\ll 1$ in (3.13) and (3.14), one can readily derive useful asymptotic solutions to (3.11)–(3.14) of the form

$$\left.\begin{aligned} &A_1=A_1^{(1)}E_1^{-1}+\ldots, \quad B_1=B_1^{(0)}+B_1^{(1)}E_1^{-1}+\ldots,\\ &A_2=A_2^{(0)}+A_2^{(1)}E_2+\ldots, \quad B_2=B_2^{(1)}E_2+\ldots \end{aligned}\right\} \tag{3.17}$$

and

$$\alpha_k=\alpha_k^{(0)}+\ldots,$$

where the coefficients $A^{(m)}, B^{(m)}, \alpha^{(m)}$ shown explicitly are all $O(1)$ for $R\to\infty$. In this way we find from (3.11)–(3.14) and (3.16) that the leading terms in (3.17) are given by

$$\left.\begin{aligned} \alpha_1^{(0)}&=\frac{(\beta_1-\beta_2)\lambda+(2\beta_1+1)}{1+\lambda},\\ A_1^{(1)}&=\tfrac{1}{2}\mathrm{i}\left\{\frac{(\beta_2-\beta_1+1)\lambda-2\beta_1}{1+\lambda}\right\},\\ B_1^{(0)}&=-\tfrac{1}{2}\mathrm{i}\lambda\left\{\frac{\beta_1+\beta_2+1}{1+\lambda}\right\}, \end{aligned}\right\} \tag{3.18}$$

with similar expressions for the set $\{-\alpha_2^{(0)}, -B_2^{(1)}, -A_2^{(0)}\}$ obtained from those given here for $\{\alpha_1^{(0)}, A_1^{(1)}, B_1^{(0)}\}$, respectively, by means of permutations $\lambda\to\lambda^{-1}, \beta_1\rightleftharpoons\beta_2$, which is dictated by the underlying symmetry of the problem.

The above asymptotic solutions for the parameters $\{\alpha_k, A_k, B_k\}$ reveal the boundary-layer structure of the system for large R, wherein one has asymptotic solutions for (3.9) and (3.10) of the form

$$\phi=\text{const}\,\mathrm{e}^{-(1+\mathrm{i})|\zeta-\hat{\zeta}|+\frac{1}{2}\mathrm{i}\alpha^{(0)}}, \tag{3.19}$$

with boundary-layers near the interface $\hat{\zeta}\equiv 0$ or the disks $\hat{\zeta}=\hat{\zeta}_i\equiv\xi_i R^{\frac{1}{2}}$, respectively, separated by an inviscid rotating core in which

$$\phi\to\tfrac{1}{2}\mathrm{i}\alpha^{(0)}, \quad \text{for } |\zeta-\hat{\zeta}|\to\infty, \tag{3.20}$$

all of which corresponds to the structure envisaged by Batchelor (1951) for the case of homogeneous fluids. Accordingly, we have also confirmed the results (3.18)–(3.20)

by a boundary-layer analysis which includes the appropriate matching in the inviscid cores and at the interface. We note that for $R \to \infty$ the asymptotic velocity distributions are given in terms of the parameters in (3.18)

$$\left.\begin{aligned} &F_1 \to 0, \quad G_1 \to \tfrac{1}{2}\alpha_1^{(0)} + 1, \quad H_1 \to B_1^{(0)} \\ \text{and} \quad &F_2 \to 0, \quad G_2 \to \tfrac{1}{2}\alpha_2^{(0)} + 1, \quad H_2 \to -A_2^{(0)} \end{aligned}\right\} \tag{3.21}$$

in the inviscid regions.

In the discussion of §5, we shall compare the results of the linearized analysis with the appropriate numerical solutions to the full nonlinear equations in (2.3).

4. Inviscid cells and multiplicity

By means of the transformation

$$f(\zeta) = R^{\frac{1}{2}} g(\xi), \quad H(\zeta) = R^{\frac{1}{2}} h(\xi) \tag{4.1}$$

of (3.1) and (3.2), one can cast (3.3) into the form

$$R^{-1} g''' + 2\,\mathrm{Re}\{g\}\, g'' - C - g'^2 = 0, \tag{4.2}$$

where primes on g denote derivatives with respect to ξ. For $R \to \infty$ the inviscid (Euler) limit is obtained in the usual way by dropping the term in R^{-1}. As shown by Dijkstra (1980), a fundamental solution to the resulting inviscid equation is, up to an arbitrary, additive imaginary constant,

$$g(\xi) = \kappa^{-1}[(1 \pm \mathrm{i}\kappa\xi)\, \Gamma + A\, \mathrm{e}^{\pm \mathrm{i}\kappa(\xi - \xi_0)}], \tag{4.3}$$

with

$$g'(\xi) = f'(\zeta) = F + \mathrm{i}G = \pm \mathrm{i}[\Gamma + A\, \mathrm{e}^{\pm \mathrm{i}\kappa(\xi - \xi_0)}] \tag{4.4}$$

and

$$h = -\frac{2}{\kappa}(\pm G) = -\frac{2}{\kappa}[\Gamma + A\cos\kappa(\xi - \xi_0)], \tag{4.5}$$

where

$$\Gamma = (A^2 + C)^{\frac{1}{2}}, \quad \text{with } A^2 + C \geqslant 0. \tag{4.6}$$

The parameters A, the amplitude; $\kappa \equiv kd$, the non-dimensional wavenumber; and $\kappa\xi_0$, the phase, are arbitrary real constants.

The expressions (4.3)–(4.6) represent a train of inviscid, rotational Euler cells or eddies, consisting of a stationary simple-harmonic disturbance superimposed on a rigid-body rotation and translation given by Γ in (4.5). In fact, (4.5) represents the solution to the relevant similarity form of the celebrated Long equation (Batchelor 1967, p. 546; Yih 1980, p. 339):

$$G'' + \kappa^2 G = \kappa^2 \Gamma. \tag{4.7}$$

As discussed below, the associated eigenvalue problem gives rise to one type of inviscid multiplicity.

The relative magnitudes of the parameters A^2 and C determine the nature of the eddy structure (4.3). Thus, for $C > 0$, rotation tends to be dominant and neither h nor G vanishes, whereas for $-A^2 \leqslant C \leqslant 0$, one has closed eddies with periodic stagnation points at which both $h = G = 0$. One extreme of this regime, $C = -A^2$, gives a purely harmonic disturbance, whereas the other represents the neutral case $C = 0$. The latter involves critical points, at which h and F vanish simultaneously, and represents the type of eddy shown by Kuiken (1971) to describe the inviscid blow-off zone for strong injection into (Kármán-type) flow above a rotating porous disk. In terms of the normal injection velocity V and rotational speed ω at the disk,

we recall that strong injection or blowing corresponds to large values of $V^2/\omega\nu$, equivalent to $\eta^2 R \gg 1$ in the present notation, and that the wavenumber of the associated inviscid eddy is

$$k = \frac{2\omega}{V} \tag{4.8}$$

in accordance with (4.5).

Subject to certain inviscid compatibility conditions, any two distinct solutions of the type (4.3) can in principle be joined at a singular surface representing a viscous interlayer for (4.2) or (3.3). In the case of a homogeneous fluid we require, for compatibility, the continuity of the pressure coefficient C and normal velocity $h = w/\omega d$, whereas at any stationary singular surface that is also a surface of stratification between different fluids we demand continuity of ρC and the vanishing of h, in accordance with the remarks following (2.5).

The above inviscid matching allows generally for the existence of a vortex sheet or a critical layer where g', as given by (4.4), or g'' are discontinuous, which leads through (4.2) to a transcendental viscous interlayer of thickness $R^{-\frac{1}{2}}$. However, for homogeneous fluids, Dijkstra (1980) and others (see Zandbergen & Dijkstra 1987) have surmised from extensive numerical studies that the typical large-R structure consists of a chain of nearly stagnant Euler cells connected, algebraically to leading order, at certain inviscid critical points by weak viscous interlayers of thickness $R^{-\frac{1}{3}}$. We note, incidentally, that the algebraic form involved is a quadratic in ξ, satisfies, therefore, both (4.2) and its inviscid form, and represents a long-wave limit of (4.3) for $\kappa \to 0$.

In light of the above remarks, it appears that the well-known multiplicity for rotating-disk flow can be traced to at least two sources, one being the non-uniqueness of 'monochromatic' (constant-κ) Euler cells corresponding to the eigensolutions of (4.7), and the other arising from various 'polychromatic' stackings of cells having different wavenumber but exhibiting inviscid compatibility (Zandbergen & Dijkstra 1987).

In the present work, we anticipate a similar eddy structure within the homogeneous-fluid layers, with a concomitant multiplicity of solution. However, because the stand-off distance or cell wavelength implied by (4.8) increases with V, we believe that the effects of injection will tend to eliminate polychromatic multiplicity at sufficiently large values of both injectional Rossby numbers η_1 and η_2. Also, we suspect that the effects of strong injection combined with stratification will in general give rise to a (Prandtl) interlayer with the standard $R^{-\frac{1}{2}}$ thickness at the interface $\xi = 0$.

For the present purposes, we focus attention on the structure for $R \to \infty$ and the inviscid matching of Euler cells at $\xi = 0$. To be definite, we assume a monochromatic Euler cell structure in either fluid, satisfying the boundary conditions (2.5) at the disk and the inviscid compatibility conditions at the interface $\xi = 0$. For each fluid layer this leads by (4.5) to a relation of the form (4.8) together with the following equations for the corresponding constants A and C:

$$\left.\begin{aligned} A^2 = \frac{\gamma^2}{4\sin^4\chi}, \quad C = -\gamma^2\cot^2\chi, \\ \text{where} \qquad \chi = \frac{\omega d}{V} \end{aligned}\right\} \tag{4.9}$$

is an inverse Rossby number and where two distinct sets of equations are understood, with subscripts $i = 1, 2$ affixed acordingly to all the quantities appearing in (4.9). By

restricting the magnitude of χ to $\frac{1}{2}\pi$, one covers the parameter range $-1 \leqslant C/A^2 \leqslant 0$ exactly twice and allows for large injection rates, where $\chi \to 0$. At the other extreme represented by $\chi = \frac{1}{2}\pi$, one has $C = 0$ and a characteristic wavelength $2\pi k^{-1}$ exactly twice the given fluid-layer thickness (d_i); whereas the mid-point $\chi = \frac{1}{4}\pi$ corresponds to $C = -A^2$ and a wavelength four times the layer thickness. We suggest here that the parameter ranges $0 \leqslant \chi \leqslant \frac{1}{4}\pi$ and $\frac{1}{4}\pi \leqslant \chi \leqslant \frac{1}{2}\pi$ serve roughly to identify within the regime of dominant injection $C < 0$ two subregimes, namely, a regime of very strong injection, where $|C| \geqslant \gamma^2$, and a regime of moderately strong injection where $|C| \leqslant \gamma^2$. Accordingly, the limit point $\chi = \frac{1}{2}\pi$, $C = 0$, serves to represent a lower bound, $2|\omega|d/\pi$, on the magnitude of the injection rate V, below which we expect to find one or more solution branches having a broad regime in Rossby number η such that $C \approx 0$ for sufficiently large $\eta^2 R$. Based on the numerous previous studies, we expect this 'neutral' regime to be characterized by multiple-cell structures and a high degree of multiplicity in a given fluid layer.

In the regime of dominant injection, $C < 0$, further light can be shed on the question of multiplicity by means of the following considerations. In addition to (4.9), the matching of ρC at $\xi = 0$ yields a key relation

$$\rho_1 \omega_1^2 \cot^2 \frac{\omega_1 d_1}{V_1} = \rho_2 \omega_2^2 \cot^2 \frac{\omega_2 d_2}{V_2} \tag{4.10}$$

connecting rotational speeds and injection rates.

As one indication of multiplicity, we note that if the Rossby number for one fluid layer, say, $V_1/\omega_1 d_1$, is chosen equal to the critical value $2/\pi$, corresponding to $C = 0$, then (4.10) indicates that the other, $V_2/\omega_2 d_2$, must assume the same critical value, or any one of the smaller values, $2/3\pi, 2/5\pi, \ldots$, representing multiple cells in that layer.

As shown below, there also exist multiplicities for the case $C < 0$, other than those associated with the sense of rotation. First it is worth noting that for large values of both Rossby numbers, corresponding to strong injection into both layers, the asymptotic form of (4.10) yields

$$\frac{\rho_1 V_1^2}{d_1^2} = \frac{\rho_2 V_2^2}{d_2^2}, \tag{4.11}$$

exactly as required by the pressure matching of opposing stagnation flows with prescribed normal velocities at the disks.

The limiting solution (4.11) suggests immediately another multiplicity for $C < 0$, arising from a related special solution to (4.10). In particular, with the parameters in fluid 2 given, we can take $\omega_1 \to 0$ in (4.10), to obtain

$$\frac{\rho_1 V_1^2}{d_1^2} = \rho_2 \omega_2^2 \cot^2 \frac{\omega_2 d_2}{V_2}, \tag{4.12}$$

corresponding to a stagnation flow in fluid 1 with infinite cellular wavelength and with a pressure field that matches that in fluid 2. We note by (4.11) that the right-hand side of (4.12) serves then to define an effective stagnation-flow parameter V/d for fluid 2.

The special case (4.12) is obviously coextant with any other solutions to (4.10) for $\omega_1 \neq 0$ and, to investigate the other possibilities, we note that (4.10) can be cast into the form

$$q\chi = \tan\chi, \tag{4.13}$$

where

$$q = \pm\left(\frac{\rho_1}{\rho_2}\right)^{\frac{1}{2}} \left|\frac{\eta_1}{\eta_2}\right| \left(\frac{d_2}{d_1}\right) \left(\frac{\tan\chi_2}{\chi_2}\right), \quad \chi \equiv \chi_1 \tag{4.14}$$

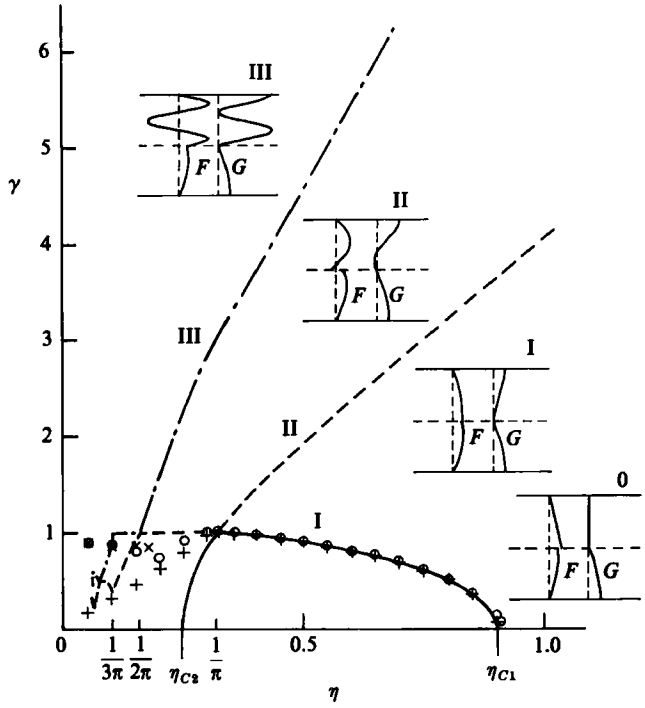

FIGURE 1. Rotation ratio $\gamma = \gamma_1 = \omega_1/\omega_2$ *vs.* injectional Rossby number $\eta \equiv \eta_2 = -\eta_1 \equiv V/\omega_2 d$ for $\rho_1/\rho_2 = 0.8$. Inviscid-cell solutions: Branch 0 ($\chi = 0$) is discrete set of points, $\eta = \eta_{C1}, \eta_{C2}, \ldots$, on $\gamma = 0$; ——, Branch I, ($\chi = X_1$); – – – –, Branch II ($\chi = X_2$); –·–·–, Branch III ($\chi = X_3$). Insets represent inviscid velocity profiles for $\eta = 0.5$ for Branches I–III. Computations are shown by: ○, $R_1 = 500$; + or ×, representing different branches, $R_1 = 5000$.

and where, as implied in (4.9), $\chi_i = \omega_i d_i/V_i$ for $i = 1, 2$. Thus, with ρ_1/ρ_2, η_1/η_2, d_2/d_1 and the parameter χ_2 specified, (4.13) provides an equation for χ_1 and, hence, for

$$\gamma_1 \equiv \frac{\omega_1}{\omega_2} = \pm \frac{\eta_1}{\eta_2}\frac{d_2}{d_1}\frac{\chi_1}{\chi_2}. \tag{4.15}$$

Equation (4.13) for $\chi(q)$, which is associated with a well-known eigenvalue problem for (4.7), is known to possess a countably infinite set of solutions, which we denumerate here as $\chi = X_0 \equiv 0, \pm X_1, \pm X_2, \ldots$, with $2X_m/\pi$ lying in the interval $(m-1, m)$ for $m = 1, 2, \ldots$, corresponding to $(-1)^m q < 0$. This solution set represents monochromatic inviscid multiplicity, in which each $m = 1, 2, \ldots$, corresponds to a cell structure in fluid 1 having wavenumber $k = 2X_m/d_1$ and, therefore, $(m-1)$ zeros of $F(\xi)$ in $\xi = (0, \xi_1)$.

For $|q| \leqslant 1$, the single-cell solution X_1 is lost, and for $|q| < 1$ one also loses the infinite-wavelength solution $\chi = 0$ whenever injection velocities and fluid depths are not compatible with (4.11).

Some of the above points become clearer in the special case to be considered at length in the present work, $\eta_2 = -\eta_1 = \eta \geqslant 0$, and $d_1 = d_2 = \frac{1}{2}d$, for which

$$\chi_2 = \frac{1}{2\eta}, \quad \chi = \frac{\gamma_1}{2\eta}, \quad q = \pm\left(\frac{\rho_1}{\rho_2}\right)^{\frac{1}{2}}\left(2\eta \tan\frac{1}{2\eta}\right) \tag{4.16}$$

in (4.14). Hence, it becomes evident that the single-cell solution is lost for Rossby

numbers η such that $|q| < 1$. Inspection of (4.14) shows that the infinite-wavelength stagnation flow $\chi = 0$ represents an acceptable solution only for discrete values of η, say $\eta_{C1} > \eta_{C2} > \ldots$, for which $|q| = 1$ in (4.16).

Figure 1 shows a plot of γ versus η, together with the representative inviscid velocity profiles given by (4.4) and (4.5) for the first four solution branches $\chi = 0, X_1, X_2, X_3$ of (4.13) and (4.14), with a density ratio $\rho_1/\rho_2 = 0.8$. Here, the two corresponding, largest discrete values of η for $\gamma = 0$ are given by $\eta_{C1} \doteq 0.89786$ and $\eta_{C2} \doteq 0.25090$. We note that the single-cell branch X_1 merges with the infinite wavelength branch $\chi = 0$ at η_{C1} and η_{C2}. We have not attempted to represent the details of the higher branches $X_2, X_3, \ldots$, for small η, since these become increasingly complex as $\eta \to 0$. In the following section, we shall compare the inviscid results with numerical solutions to the full equations.

5. Numerical computations, comparisons and conclusions

Subject to the subsidiary conditions listed above, the differential equations (2.3) were treated by a finite-difference numerical scheme based on an existing computer-library subroutine, ('DVCPR', from International Mathematics and Statistics Library Inc. Reference Manual, 1982) for the solution of two-point boundary-value problems.† The subroutine is based on a Newton–Raphson iteration, with adjustable step size to handle 'stiff' equations of the type arising for large R in (2.3). To treat the latter, we have cast them into a standard first-order vector equation in $\mathrm{d}/\mathrm{d}\xi$, containing component equations of the type

$$\frac{\mathrm{d}C}{\mathrm{d}\xi} = 0 \tag{5.1}$$

for the constant parameters. Also, to satisfy the normal-velocity condition $H = 0$ at $\xi = 0$, we introduce a 'false' variable K, such that

$$\frac{\mathrm{d}K}{\mathrm{d}\xi} = \begin{cases} 0, & \text{for } \xi > 0, \\ \dfrac{\mathrm{d}H}{\mathrm{d}\xi}, & \text{for } \xi < 0, \end{cases} \tag{5.2}$$

with

$$K = 0, \quad \text{at } \xi = \xi_1 = \frac{d_1}{d}$$

and

$$K = H_2, \quad \text{at } \xi = \xi_2 = -\frac{d_2}{d}, \tag{5.3}$$

in this way converting the interfacial condition to a two-point boundary-value problem. (A seven-dimensional vector space is ultimately required.)

Where possible, we have tested our computations against those of previous work (Lance & Rogers 1962; Holodniok *et al.* 1977, 1981) for the special case of a homogeneous fluid with no injection, in which 'custom-made', as opposed to our 'off-the-shelf' software was employed. As judged from comparisons of graphical velocity profiles for the case $\gamma_1 = -1$, the quantitative agreement between identical types of solutions appears satisfactory. However, in distinction to the work of Holodniok *et al.* (1981), we did not encounter parametric singularities nor did we generate multiple solutions. We believe this to be due to the limited nature of our

† Detailed numerical results as well as a listing of our computer algorithm are available on request from the authors.

exploratory numerical work. We have also carried out computations for the special cases $\eta_1 = \eta_2 = 0$ and $\gamma_2 = -\gamma_1 = 1$, with various combinations of $R_1 = 1, 50$, $\rho_2/\rho_1 = 1, 3$ and $\mu_2/\mu_1 = 0.4, 1, 3$, considered in the previous work of Pécheux & Boutin (1985) on stratified two-disk flow. By starting our computations with $\gamma_2 = 1$ and their graphically reported values of liquid depth ξ_1, we find $\gamma_1 \doteq -1$, as required, except for the larger Reynolds number $R_1 = 50$ and extreme density ratio $\rho_2/\rho_1 = 3$, where the computed values of γ_1 were so sensitive to ξ_1 as to preclude meaningful comparison. While this may suggest parametric singularities, we have not explored the issue in depth.

With a view towards eventual experimentation, and in order to illustrate certain important qualitative features, most of our numerical computations have been executed for fluid-property ratios typical of a water/light-oil ('kerosene' or aviation jet fuel) system $\rho_1/\rho_2 = 0.8$ and $\mu_1/\mu_2 = 2.5$. Also, we have chosen $V_2 = -V_1 \geqslant 0$ and $d_1 = d_2$ for purposes of exploratory computations. Figures 2–9 provide a graphical summary of some of the highlights of our computations. In the absence of experiment or of stability considerations, the results shown for the extremely large Reynolds numbers of 10^4 should perhaps be regarded more a matter of computational facility than a reflection of physical reality.

Since our density ratio of 0.8 is not too far removed from unity, the theory developed for nearly-rigid rotation turns out to work rather well for the case of corotating disks. This is illustrated in table 1, where we compare certain salient aspects of the numerical solutions to (2.3) with the linearized theory, both that obtained for general R_1 by numerical solution of the algebraic equations (3.11)–(3.15) and, for large R_1, by the associated boundary-layer analysis. Although not shown here, we note that for zero injection at the disks the linearized theory gives a quite satisfactory description of the eddy structure. The theory also displays another remarkable feature of the numerical results, namely, that the fluid interface behaves essentially as a rigid solid. Computed values of the nominal perturbation parameter ϵ of (3.4) are also shown in the table. As can be seen, the linearized theory is quite good even for relatively large values of ϵ as long as the injection rate is small. In particular, for values of the injection velocity $-H_1 \lesssim 0.01$ it is evident that injection begins to disrupt the nearly-rigid rotation.

We also note that, with the exception of a very weak flow in figure 2 (*a*), the results in figures 2–5 do not indicate simultaneous flow patterns of the Kármán type near the interface, with flow directed toward the interface in both fluids. To achieve such a pattern it appears necessary to introduce injection as discussed above.

Figures 6–8 show a rather rich eddy structure resulting from the combination of rotation and injection, for the special case of equal injection rates $V_2 = -V_1 > 0$. We believe this structure reflects a high-R state, consisting of multiple inviscid cells interspersed with viscous interlayers, of the type that has been discussed theoretically by Kuiken (1971), Ockenden (1972), Dijkstra (1980) and Zandbergen & Dijkstra (1987) and that is evident in the numerical solutions of Dijkstra (1980), Keller & Szeto (1980), and of Holodniok *et al.* (1981) for homogeneous fluids. One discerns from the figures that injection becomes rapidly dominant with increasing Rossby number $V/\omega d$, giving rise to stagnation-type streamlines and a flow pattern that is considered by us to be essential for achieving a uniformly accessible interface.

The computations shown in figure 9 indicate the effects of further increasing injection, until we achieve the regime of strong injection identified in §4 for inviscid flow. At the Reynolds number $R_1 = 500$, represented in figure 9, the structure predicted from the inviscid theory of §4 is already evident, although the viscous

			$G-1$											
			Lower core			Interface			Upper core			Upper disk		
$-H_1$	R_1	ϵ	LA	L	N	LA	L	N	LA	L	N	LA	L	N
0	10	0.2237		0.0837	0.0795		0.1609	0.1563		0.2059	0.2003		0.2519	0.2453
	100	0.2265		0.0746	0.0719		0.1497	0.1476		0.2026	0.1991		0.2554	0.2516
	1000	0.2265	0.0748	0.0748	0.0721	0.1497	0.1496	0.1474	0.2025	0.2025	0.1987	0.2555	0.2554	0.2514
0.01	10	0.2156		0.0656	0.0629		0.1402	0.1380		0.1877	0.1849		0.2417	0.2383
	100	0.2133		0.0534	0.0526		0.1261	0.1270		0.1766	0.1770		0.2388	0.2400
	1000	0.2134	0.0536	0.0536	0.0527	0.1240	0.1260	0.1268	0.1771	0.1771	0.1771	0.2388	0.2389	0.2398
0.05	10	0.1836		−0.0054	0.0024		0.0587	0.0704		0.1169	0.1295		0.2022	0.2149
	100	0.1595		−0.0300	−0.0201		0.0330	0.0493		0.0739	0.0934		0.1733	0.1968
	1000	0.1597	−0.0296	−0.0296	−0.0195	0.0329	0.0330	0.0494	0.0771	0.0773	0.0963	0.1735	0.1736	0.1966
0.1	10	0.1444		−0.0911	−0.0615		−0.0398	−0.0015		0.0318	0.0730		0.1556	0.1946
	100	0.0898		−0.1309	−0.1021		−0.0796	−0.0376		−0.0504	−0.0006		0.0940	0.1490
	1000	0.0905	−0.1302	−0.1302	−0.1001	−0.0795	−0.0794	−0.0368	−0.0437	−0.0435	0.0062	0.0945	0.0948	0.1492

TABLE 1. Comparison of $G-1$ from linear approximation (L) and linear asymptotic approximation for large Reynolds number R_1 (LA) with numerical calculation (N) for various Reynolds numbers R_1 and injection rates $H_1 = (V_1/d\omega_2)R_1^{\frac{1}{2}}$ with $-V_1 = V_2 > 0$

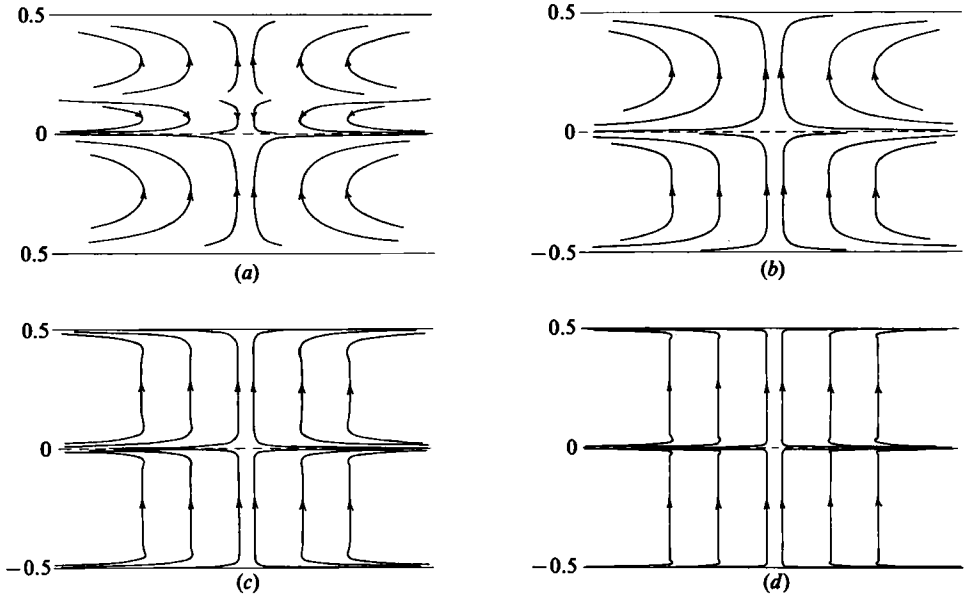

FIGURE 2. Streamlines of corotational flow without injection ($\eta_1 = \eta_2 = 0$) at various Reynolds numbers $R_1 = d^2\omega_2/\nu_1$: (*a*) 10, (*b*) 100, (*c*) 1000, (*d*) 10000.

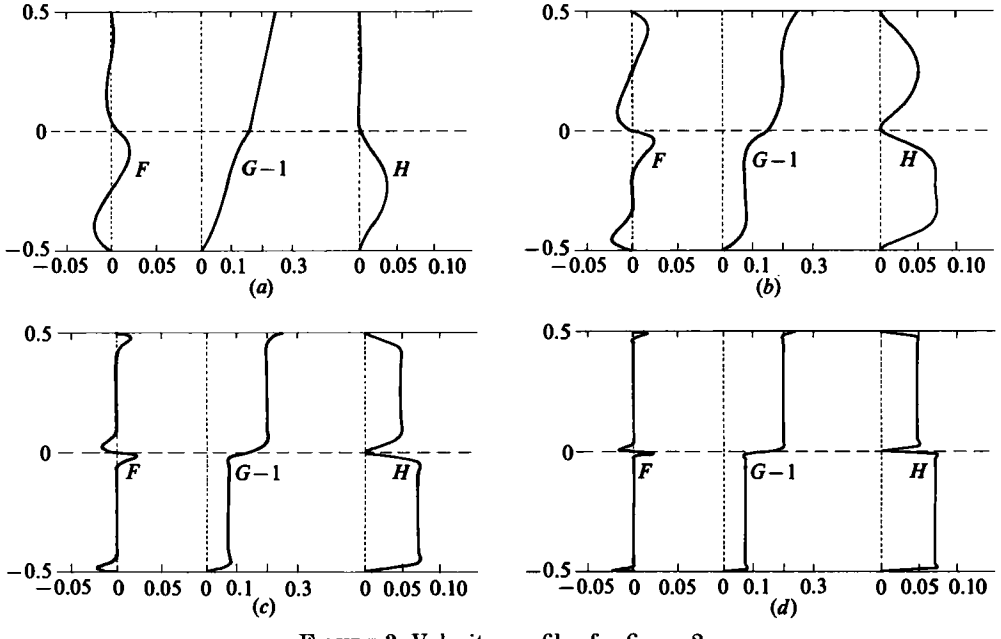

FIGURE 3. Velocity profiles for figure 2.

interlayers are still quite prominent. In order to compare this more closely with inviscid theory, we have carried out computations for a much larger Reynolds number $R_1 = 5000$. Although not shown here, the velocity profiles for $\eta \geqslant 1/\pi$ are virtually indistinguishable from the inviscid single-cell ($m = 1$) solutions discussed in §4.

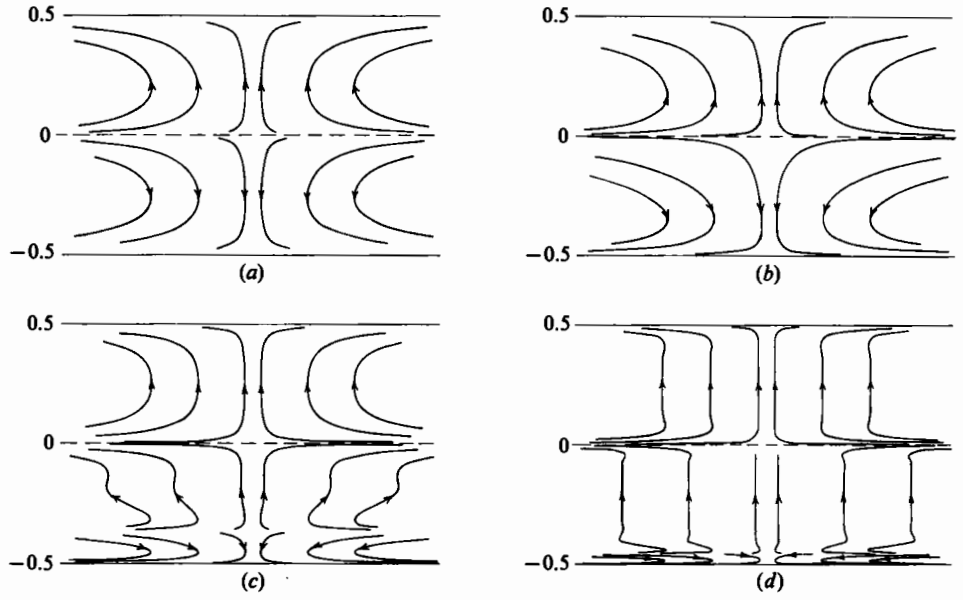

FIGURE 4. Streamlines for counter-rotational flow without injection at various R_1: (*a*) 10, (*b*) 100, (*c*) 1000, (*d*) 10000.

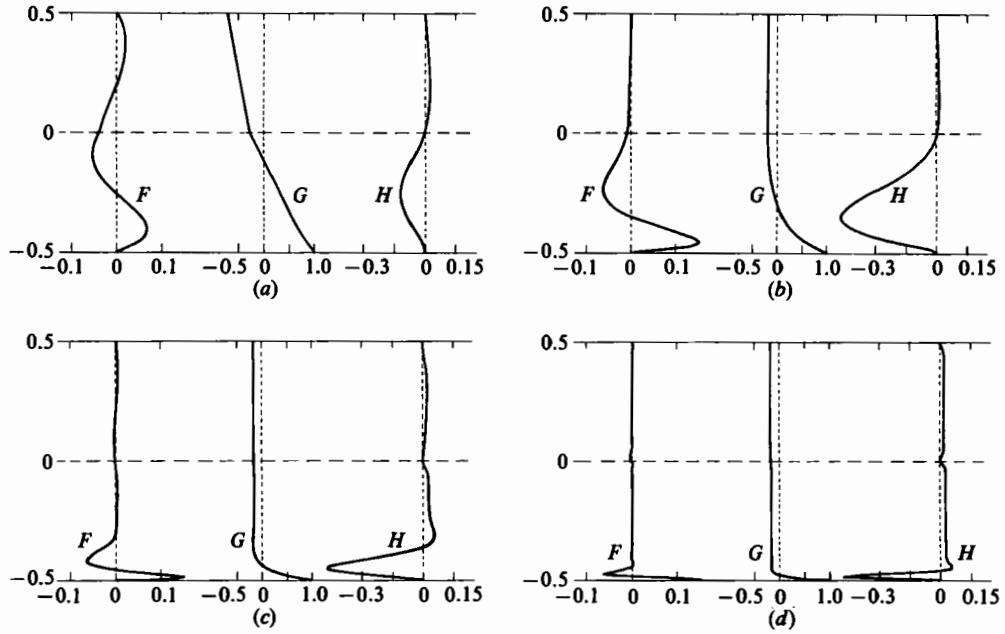

FIGURE 5. Velocity profiles for figure 4.

The corresponding computations for the speed ratio $\gamma \equiv |\gamma_1| = |\omega_1/\omega_2|$ are shown in figure 1 for Rossby numbers η in the range of 0.1 to $\eta_{C1} \doteq 0.89786$. Once again, in the inviscid strong-injection regime, $\eta_{C1} > \eta \geqslant 1/\pi$, the computations are virtually indistinguishable, both for $R_1 = 500$ and $R_1 = 5000$, from the inviscid theory for $m = 1$. As can be seen from figure 9(*d*), one approaches the infinite-wavelength state

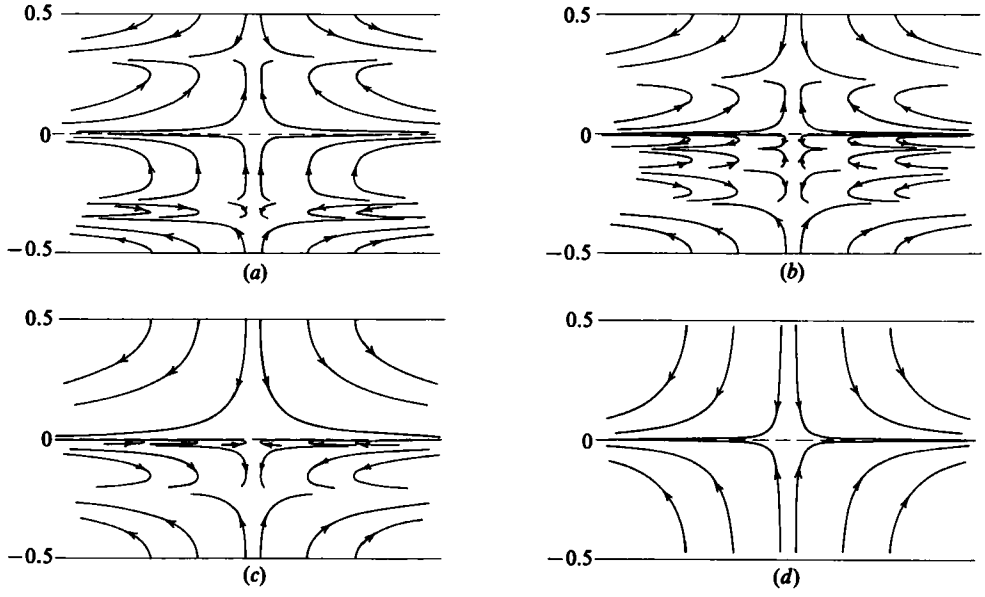

FIGURE 6. Streamlines for corotational flow with injection at $R_1 = 500$ and various injection velocities $\eta \equiv \eta_2 = -\eta_1 \equiv V/\omega_2 d$: (*a*) 0.056, (*b*) 0.11, (*c*) 0.17, (*d*) 0.22.

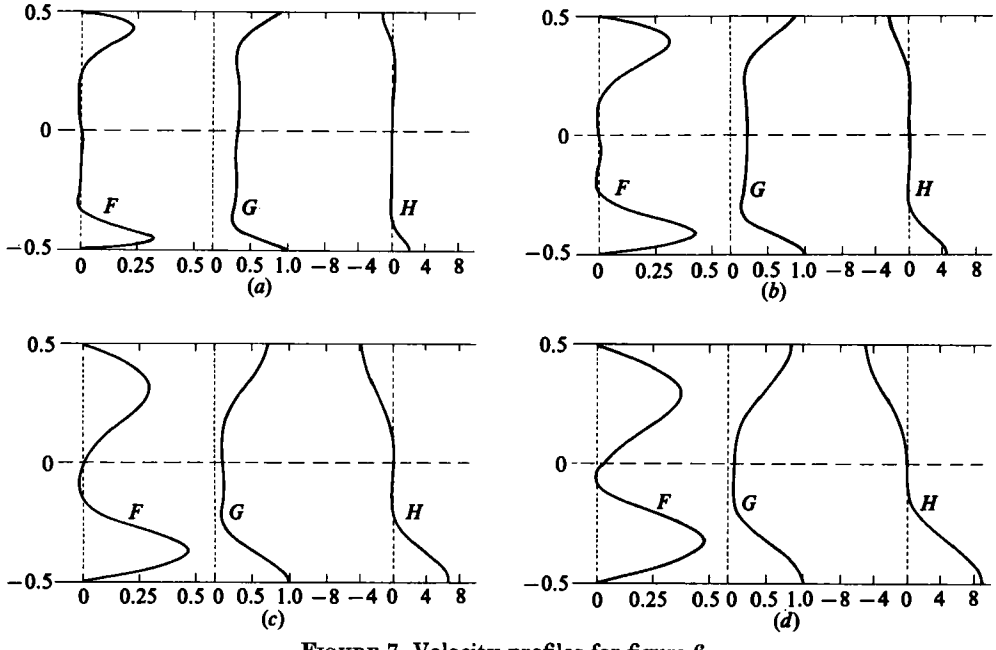

FIGURE 7. Velocity profiles for figure 6.

$m = 0$ for $\eta \to \eta_{C1}$. However, for very strong blowing, at or above the terminus of the $m = 1$ inviscid branch, $\eta \geqslant \eta_{C1}$, we were never able to obtain convergence in our numerical computations. Unfortunately, our present continuation methods are not adequate to get us onto one of the higher branches, shown for $m = 2, 3$ in figure 1.

For $\eta < \eta_{C2} \doteq 0.25090$ we were able to generate multiple solutions numerically for

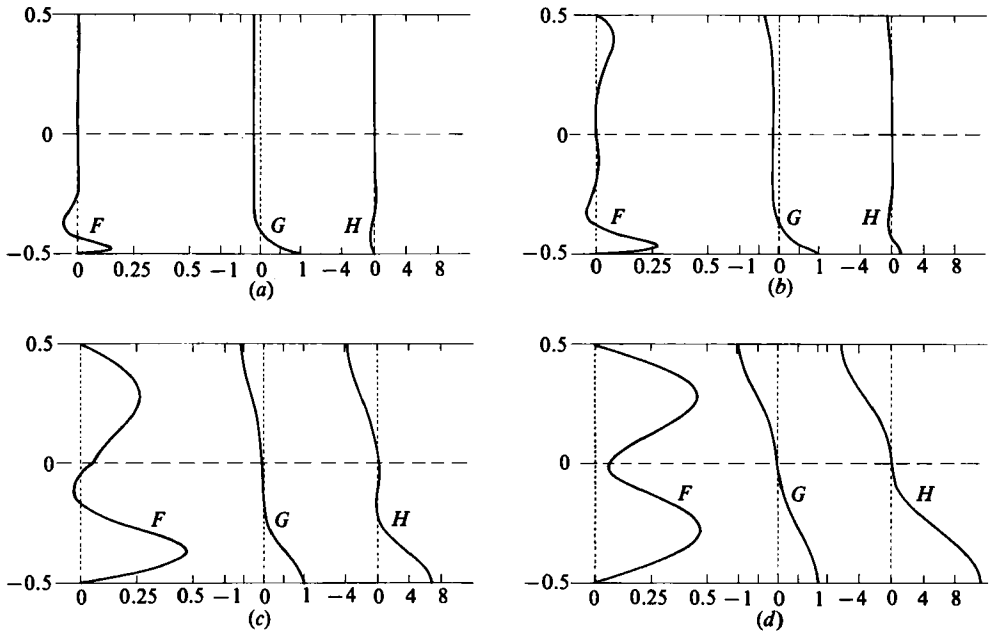

FIGURE 8. Velocity profiles for counter-rotational flow with injection at $R_1 = 500$ and various η: (*a*) 0, (*b*) 0.028, (*c*) 0.17, (*d*) 0.28.

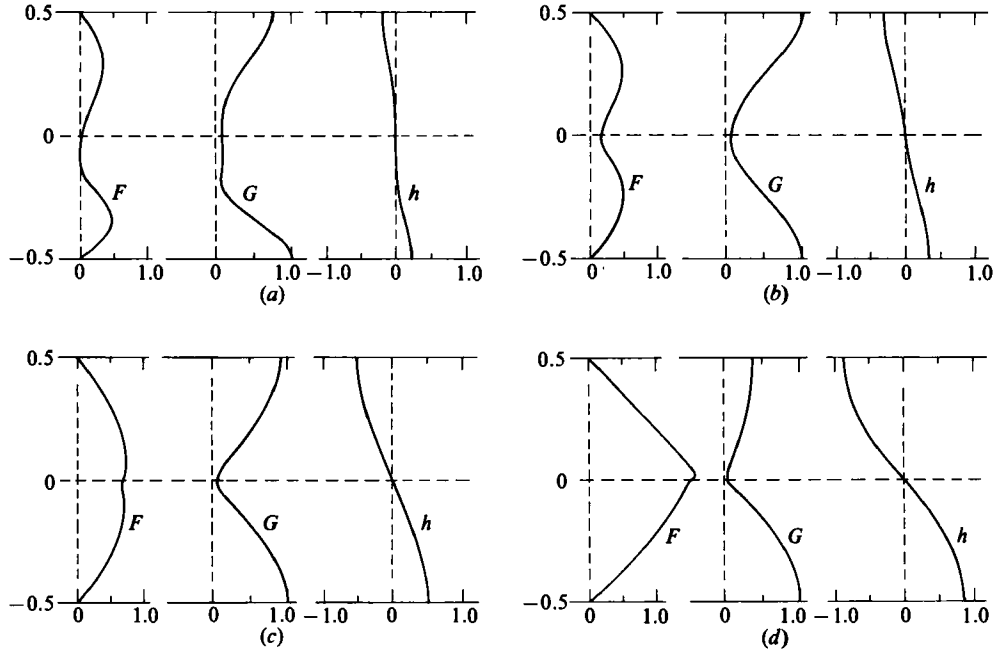

FIGURE 9. Velocity profiles for corotational flow at $R_1 = 500$ and various η: (*a*) 0.20, (*b*) $0.32 \approx 1/\pi$, (*c*) 0.5, (*d*) 0.85.

$R_1 = 5000$, as indicated in figure 1. We therefore believe that polychromatic cell structure and multiplicity is involved for $\eta < 1/\pi$ but have not explored this in detail.

While not shown here, we find that a plot of the pressure coefficient C_1 versus η for $R_1 \geqslant 500$ has $C_1 \approx 0$ for $\eta < 1/\pi$, in line with our conjecture of §4, and

$$C_1 = -\frac{\rho_2}{\rho_1} \cot^2\left(\frac{1}{2\eta}\right)$$

for $\eta_{C1} > \eta \geqslant 1/\pi$, exactly as predicted by the inviscid theory.

In conclusion, our computations and the inviscid theory presented above suggest that injection not only serves to generate the type of flow pattern desired, but it also tends to reduce multiplicity and the associated complexity of the similarity-solution structure. It seems to us evident that injection would also have the further benefit, for the applications envisaged here, of minimizing the edge effects that must be present with any finite disk system and which are predicted by Brady & Durlofsky (1987) to persist even in the limit of infinite disks for the case of no injection.

Therefore, the above type of rotational system offers promise for generating a uniformly accessible fluid–fluid interface, with potentially more flexibility than non-rotational stagnation flow. This, together with some of the fluid-mechanical questions raised above, appears worthy of further investigation.

The authors wish to acknowledge support from the University of Southern California, in the form of ARCS and Chevron Graduate Fellowships (to J.B.M.), a Warren T. Chow China-Scholar Fellowship (to K.Z.), and the use of computer graphics facilities in the Department of Aerospace Engineering. Part of the work was completed during the tenure of American Chemical Society Petroleum Research Fund Grant 18934-AC7 and National Science Foundation Grant CBT-8616201 (to J.D.G.). We are grateful to all the above sponsors.

REFERENCES

BATCHELOR, G. K. 1951 Note on a class of solutions of the Navier–Stokes equations representing steady rotationally-symmetric flow. *Q. J. Mech. Appl. Maths* **4**, 29.

BATCHELOR, G. K. 1967 *An Introduction to Fluid Dynamics*. Cambridge University Press.

BÖDEWADT, U. T. 1940 Die Drehströmung über Festem Grunde. *Z. Angew. Math. Mech.* **20**, 241.

BRADY, J. F. & DURLOFSKY, L. 1987 On rotating disk flow. *J. Fluid Mech.* **175**, 363.

CHAPMAN, T. W. & BAUER, G. L. 1975 Stagnation-point viscous flow of an incompressible fluid between porous plates with uniform blowing. *Appl. Sci. Res.* **31**, 223.

DIJKSTRA, D. 1980 On the relation between adjacent inviscid cell type solutions to the rotating-disk equations. *J. Engng Maths* **14**, 133.

GHIM, Y.-S. & CHANG, H.-N. 1983 Stagnation point flow in a diffusion cell. *Chem. Engng Sci.* **38**, 2067.

HOCKING, L. M. 1962 An almost-inviscid geostrophic flow. *J. Fluid Mech.* **12**, 129.

HOLODNIOK, M., KUBIČEK, M. & HLAVAČEK, V. 1977 Computation of the flow between two rotating coaxial disks. *J. Fluid Mech.* **81**, 689.

HOLODNIOK, M., KUBIČEK, M. & HLAVAČEK, V. 1981 Computation of the flow between two rotating coaxial disks: multiplicity of steady-state solutions. *J. Fluid Mech.* **108**, 227.

KÁRMÁN, TH. VON 1921 Laminare und Turbulente Reibung. *Z. Angew. Math. Mech.* **1**, 233.

KELLER, H. B. & SZETO, R. K.-H. 1980 Calculation of flows between rotating disks. In *Computing Methods in Applied Science and Engineering* (ed. R. Glowinski & J. L. Lions). North-Holland.

KUIKEN, H. K. 1971 The effect of normal blowing on the flow near a rotating disk of infinite extent. *J. Fluid Mech.* **47**, 789.

LAI, C.-Y., RAJAGOPAL, K. R. & SZERI, A. Z. 1984 Asymmetric flow between parallel rotating disks. *J. Fluid Mech.* **146**, 203.

LANCE, G. N. & ROGERS, M. H. 1962 The axially symmetric flow of a viscous fluid between two infinite rotating disks. *Proc. R. Soc. Lond.* A **266**, 109.

LEVICH, V. G. 1962 *Physicochemical Hydrodynamics*. Prentice-Hall.

MELVILLE, J. B. & GODDARD, J. D. 1985 Mass-transfer enhancement and reaction rate limitations in solid–liquid phase-transfer catalysis. *Chem. Engng Sci.* **40**, 2207.

OCKENDON, H. 1972 An asymptotic solution for steady flow above an infinite rotating disc with suction. *Q. J. Mech. Appl. Maths* **25**, 291.

PÉCHEUX, P. J. & BOUTIN, C. 1985 Étude de l'écoulement laminaire de deux liquides non miscibles entre deux disques coaxiaux tournant en sens contraires. *Z. Angew. Math. Phys.* **36**, 238.

POLLARD, R. & NEWMAN, J. 1980 Silicon deposition on a rotating disk. *J. Electrochem. Soc.* **127**, 744.

PROUDMAN, I. 1956 The almost-rigid rotation of viscous fluid between concentric spheres. *J. Fluid Mech.* **1**, 505.

SCHLICHTING, H. 1975 *Boundary-Layer Theory*. McGraw-Hill.

SMITH, K. A. & COLTON, C. K. 1972 Mass transfer to a rotating fluid: Part I. Transport from a stationary disk to a fluid in Bödewadt flow. *AIChE J.* **18**, 949.

STEWARTSON, K. 1953 On the flow between two rotating coaxial disks. *Proc. Camb. Phil. Soc.* **49**, 333.

STEWARTSON, K. 1957 On almost rigid rotations. *J. Fluid Mech.* **3**, 17.

STOWE, L. R. & SHAEIWITZ, J. A. 1981 Hydrodynamics and mass transfer characteristics of a liquid/liquid stirred cell. *Chem. Engng Commun.* **11**, 17.

YIH, C. S. 1980 *Stratified Flows*. Academic.

ZANDBERGEN, P. J. & DIJKSTRA, D. 1987 Von Kármán swirling flows. *Ann. Rev. Fluid Mech.* **19**, 465.